








Stress-Strain State of the Floating Bollard's Structure for a Shipping Gateway

Ihor Sydorenko^(✉) , Vladimir Tonkonogyi , Vladimir Semenyuk ,
Valeriy Lingur , and Yunxuan Zhang 

Odessa Polytechnic National University, 1, Shevchenko Avenue, Odessa 65044, Ukraine
igs.ods@gmail.com

Abstract. The floating ballard is one of the main elements of the mooring equipment included in the lock. The reliability of this element largely determines the performance of this complex hydraulic unit and reduces the costs associated with the accident rate of both the lock itself and the ships passing through it. The close relationship between the reliability of the bollard and the magnitude of external forces (acting on its structure) requires a deep analysis of the stress-strain state of both the bollard elements and their connection places. The article deals with studying an actual composite welded structure of a ship's lock floating bollard under short-term action of loads exceeding the nominal load due to the dynamics of mooring operations and weather conditions. The studies were carried out on the developed 3D model of the device, and the analysis of the stress-strain state of its elements and the places of their conjugation. Some simplifications were applied, and the finite element method was used. A graphical representation of the results of the study made it possible to establish a general picture of the stress-strain state of the bollard elements, as well as to establish the local places of probable damage. Based on the results obtained, appropriate conclusions are drawn that determine possible solutions to the identified problems.

Keywords: Ship lock · Mooring equipment · Floating bollard · Stress-strain state · Finite element method · Industrial growth

1 Introduction

To date, the mooring of a vessel in a lock chamber is one of the most essential operations that determine the performance and efficiency of a ship lock. That is why the mooring equipment used in this operation is subject to increased requirements in terms of its reliability. The key element of the lock's mooring equipment is the floating bollard.

The specifics of the operation of this device (in addition to the fact that it is floating) is in the nature of its loading. Many external factors determine the nature of the loading of a floating bollard. First of all, it should be noted that the mooring of ships in the lock is carried out using relatively rigid and heavy ropes. However, the ropes are elastic elements, and as a result, their stretching under load and subsequent sagging lead to significant ship movements both along and across the lock chamber. The movement

of ships is one of the leading causes of inertial jerks with a variable direction, which are perceived by the design of a floating bollard. Selective, due to the complexity of the design, the use of devices for damping inertial jerks in mooring systems does not fundamentally change the situation, and the kinetic energy of jerks remains quite large. This leads to the destruction (breakage) of the mooring ropes and the global destruction in the form of the structures of floating bollards.

It should be noted that during the locking of ships, especially heavy ones, another additional and difficult to take into account when designing a bollard loading occurs, which affects the elastically deformed state of its elements. The occurrence of this loading is often associated with two factors. The first factor in the occurrence of additional bollard exposure is the excess of the normative hydrodynamic force when filling or emptying the sluice chamber. Secondly, and no less important factor, is the unpredictable change in the mass of the moored vessel due to its freezing in the winter.

The analysis of the stress-strain state of the bollard elements under the action of the indicated loads, both at the stage of designing new devices and those in operation, is quite relevant.

2 Literature Review

The floating bollard is the main element included in almost any ship lock (Fig. 1a). The designs of such devices are quite diverse. However, despite the design differences, these devices have similar design elements that determine their functional purpose, making it possible to classify these designs as typical.

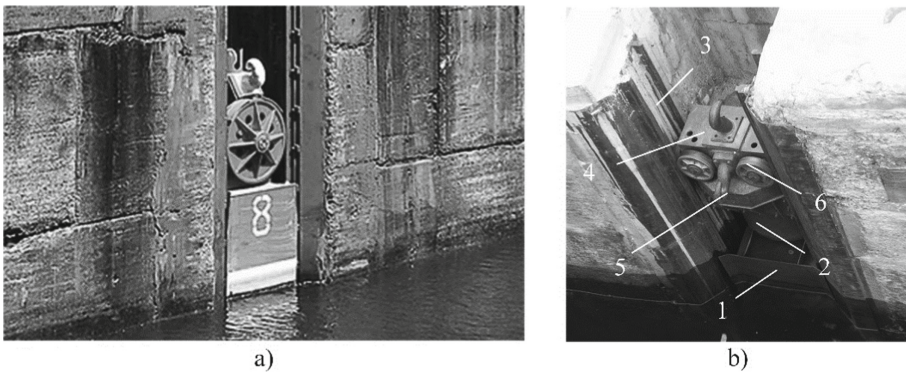


Fig. 1. Mooring equipment of the ship's lock: floating bollard (a); floating bollard elements (b)

In a typical floating bollard structure, there is always float 1, which ensures its buoyancy. Attached to the float is a metal structure 2, made of shaped profiles or sheet metal, in most cases using welding (Fig. 1b). There are designs in which the metal structure itself forms the float cavity.

In the event of a change in water level, the vertical movement of the bollard is ensured by its placement in a special shaft of the mooring pier 3. The metal structure of

the bollard, which is not part of the float, usually consists of structurally identical upper carriage 4, which is in the surface position, and the lower carriage, which is below the water level. On the upper carriage 4, for attaching the mooring piping, an eye 5 is fixedly fixed, sometimes made in the form of a hook. One or more support rollers 6, located on the upper and lower carriages, are designed to orient and hold the bollard in the pier shaft [1].

The operational experience of floating bollards indicates two main types of destruction (emergencies) that determine its complete or partial failure [2–5]. Simultaneously, the available data also indicate a precise localization of one or another type of damage in the pedestal structure. Most accidents with various technological equipment are associated with the deformation of loaded parts [6–10]. The picture of destruction, in this case, is a critical plastic deformation of the guide rollers of the bollard in the shaft, which causes the bollard to skew, and as a result, it jams. In this case, the destruction of the concrete structure of the mine is sometimes observed at the points of fastening of the guides [7]. It has been established that the presented type of bollard failure is a direct consequence of more severe damage but related directly to the bollard structure itself. 80% of accidents occur, at which the critical plastic deformation of the metal structure of the bollard (sometimes complete destruction) was recorded at the points of attachment of the eye and guide rollers on it [11, 12]. The results of the presented studies, particularly in the infrastructure development [13–16], allow us to state that the main element that determines the performance of the ship lock mooring equipment system is the bollard metal structure [17]. Based on the presented conclusions, it should be recognized that the study of the metal structure of bollards, both at the design stage and during operation, is one of the priority scientific and applied tasks.

Studies in mathematical modeling of the stress-strain state of the bollard metal structure at the design stage can significantly reduce the risk of emergencies by creating a rational bollard metal structure, and research in the process of operation makes it possible to upgrade existing equipment and thereby increase its reliability. As noted earlier, the bollard metal structure is a structure that can be classified as a combined one. The combination, in this case, contains rod, plate, or shell elements [18]. Rarely enough are metal structures assembled using only threaded or welded joints. As a rule, when assembling the metal structure of a bollard, these two types of connections are used. The bulk of the connections are welded, and the fastening of individual elements can be performed using a threaded connection [19, 20].

To analyze the stress-strain state of the considered metal structure, it is possible to use several methods known from structural mechanics. Among them, one can single out the finite difference method, the weighted residual method, variational methods, as well as the finite element method [21]. At present, the finite element method is the most common method for solving problems in the mechanics of a deformable elastic body. This method is based on the approximation of a continuous medium, which is the object of study, some simple elements interconnected at nodal points. At these points, some fictitious interaction forces are applied that characterize the action of distributed internal stresses applied along the joining boundaries of adjacent elements [21, 22].

The development of design technologies makes it possible to model the research object in a 3D model using CAD systems. Since there is a close relationship between

CAD and CAE systems, where the finite element method (FEM) has already been implemented, it is quite apparent that this method is used to conduct studies whose subject is the stress-strain state.

3 Research Methodology

The research object in this article is the existing bollard design (the most loaded upper part with an eye), which is in actual operation. The subject of the study is the stress-strain state of structural elements when external loads change in a particular range.

The range of external loads of the bollard is adopted, considering the following factors. The load on the eye of the bollard (taken during the design of the bollard), considering the stretching of the ropes and the action of the nominal hydrodynamic force on the moored vessel of the maximum allowable tonnage when opening the gates of the lock chamber $F_1 = 150$ kN, is set as the initial one. The experience of operating a lock in the spring shows that an increase in the water level in the upper cascade of the lock due to snowmelt can cause a significant increase in the nominal hydrodynamic force. When modeling such a situation, the load on the eye of the bollard is assumed to be $F_2 = 200$ kN. The operation of the lock in winter determines one more factor, which is taken into account in the simulation. Vessel icing is considered as such a factor, in which its mass increases by 20... 25% on average. This, in turn, leads to an increase in the load on the bollard eye to the value $F_3 = 300$ kN. Considering the last factor and determining the relationship between it and the stress-strain state of the bollard elements is the most important since the most significant number of damages to the considered bollard was recorded in the winter period. Other force factors, namely the gravity force of the bollard metal structure, were not considered since this device has positive buoyancy, and the gravity forces of the structure are compensated by the expulsion force of the aquatic environment acting on the float.

The CAD system Autodesk Inventor was used to creating a corresponding 3D model based on the object of study. The basis for the creation was a set of working drawings of the operated bollard (Fig. 2a), specification of the product materials and technological maps for its manufacture. In the 3D modeling of the research object, some simplifications were adopted: the lateral guide rollers 1 and 2 of the real design (Fig. 2a) in the 3D model are represented by the protrusions in the form of prisms 1 and 2, about 8 units totally (Fig. 2b). This simplification is based on the fact that damage to the guide rollers is not fixed in real situations. At this stage, the XYZ coordinate system is introduced into the model, located by the XY plane at the lower end of the structure. The Z-axis of the introduced coordinate system passes along the axis of symmetry of the structure.

Considering the structural design of the simulated metal structure and information about the fixed damages in the developed 3D model, four main elements were identified for the analysis of their stress-strain state under changing external loading (Fig. 2c). These include the upper plate 1 for fixing the eye (as the most often deformable one), which is a “kerchief” element made of rolled stainless steel sheet 1.4541 EN 10088-1:2019 with a thickness of 30 mm; top 2 and bottom 3 round covers with two segments removed, made of rolled C45 ISO 6929:1987 structural steel sheet 25 mm thick; eye 4, made of a rolled round profile of low-carbon steel E 235-C (Fe 360-C) ISO 630:1995

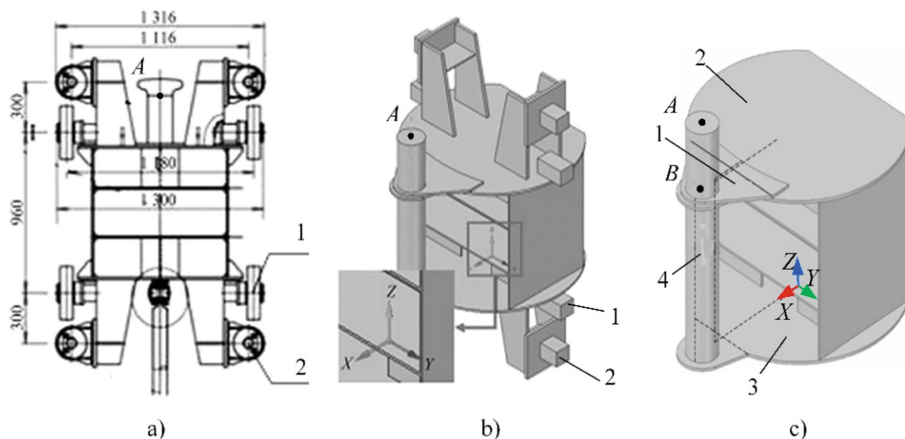


Fig. 2. Modeling of the bollard structure under study: general overall dimensions of the structure (a); 3D model with accepted simplifications and coordinate system (b); structural elements under study and binding of reference points (s)

with a diameter of 100 mm. When conducting studies of the stress-strain state of the selected elements, it was considered that external loading in the form of a mooring force is applied at the first reference point A on the eye, located at a distance of $\frac{3}{4}$ of the height of the eye from the top cover 2. The loading action is along the X-axis of the adopted system coordinates.

Analysis of the stress-strain state of the selected elements was carried out using the ANSYS Workbench CAE system after exporting the developed model from the CAD system to it. To reduce the error of geometric discretization when constructing a computational finite element mesh with one cell in the form of a cube with a side of 15 mm, adaptive mesh refinement by cells in the form of a cube with a side of 5 mm is implemented, which is used in some places of the model (the total volume of cells is increased by 18%). Adaptive mesh refinement is performed in the Solid186 block of the used CAE system. The nodes of each finite element of the computational grid of finite elements are subject to restrictions on 6 degrees of freedom, which determine their zero displacements and rotation angles.

The verification of the adequacy of the developed model and the corresponding computational finite element mesh was carried out by comparing the results of the test calculation of the bending stresses of element 4 (eye) both using the FEM and in the case of its simplified modeling by a beam with a uniform cross-section at a place determined by the second reference point B (see Fig. 2c). Simultaneously, the upper and lower elements of the “kerchief” of the bollard metal structure were considered as hinged supports of this beam, limiting its movement along the OX axis of the adopted coordinate system and making it statically determinate.

The calculated bending stresses, in this case, are obtained by the ratio of the obtained bending moments along the axis of the beam correlated to the area of its cross-section, which determines the expression

$$\sigma = M_{nz}/(W_{nz}) \quad (1)$$

where M_{nz} is the value of the bending moment in a particular section n , perpendicular to the longitudinal axis Z of the considered beam; W_{nz} is the area of the beam in some section n , perpendicular to the longitudinal axis Z of the considered beam.

The following was obtained when comparing the results of test calculations performed under the action of a load on the reference point of eye A with the value $F_1 = 150$ kN. The stresses at the reference point B are 144.9 MPa and 141.3 MPa, respectively, for the FEM and the simplified calculation version. Thus, a relative error of about 2.5% was established, which allows us to assert that the developed model of the metal structure of a floating bollard of an actual design is fully adequate and that further research is possible.

In carrying out further studies, which consisted of a series of calculations of the considered structure in the accepted range of external loads, it was possible to obtain specific results in the form of appropriate stress diagrams associated with the geometric parameters of the elements selected for the study (Fig. 3).

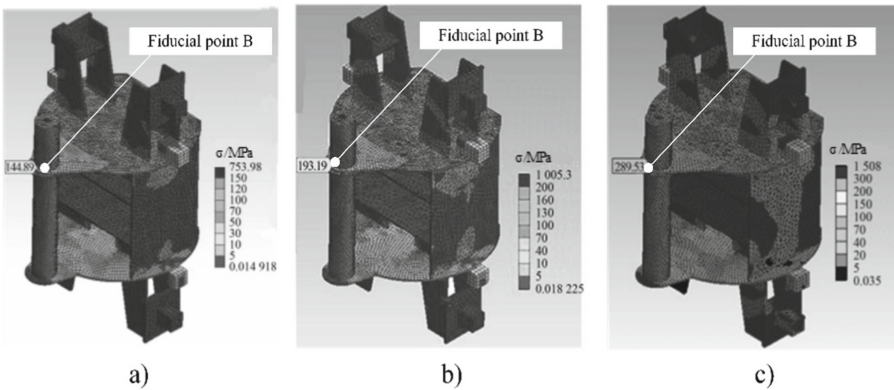


Fig. 3. Stress diagrams when modeling a bollard by the finite element method: under the action of a load F_1 on the eye (a); under the action of load F_2 on the eye (b); under the action of the load F_3 on the eye (c)

4 Results

In the course of the studies carried out, it was found that in the case of variation in the load applied at the reference point A by the values $F_1 = 150$ kN, $F_2 = 200$ kN $F_3 = 300$ kN at the second reference point B, the position of which, in the accepted coordinate system, is determined by the values $X = 715$ mm, $Y = 0$ mm, $Z = 800$ mm, corresponding stresses arise $\sigma_1 = 144.9$ MPa, $\sigma_2 = 193.2$ MPa, $\sigma_3 = 289.5$ MPa. This determines the relationship between the load change and the stresses and shows the consistency of the simulation with the actual situation.

Graphical interpretation of the calculated stress distribution diagram on element 1 “kerchief” in a plane parallel to the XY plane of the adopted coordinate system shows the following (Fig. 4a).

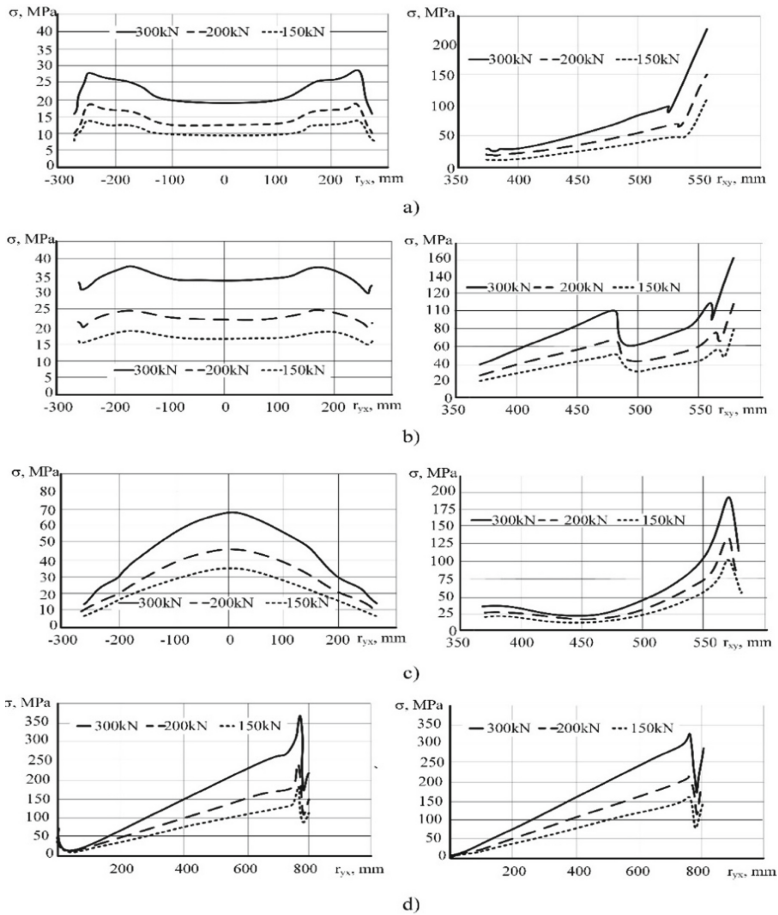


Fig. 4. Distribution of stresses in a structural elements bollard: eltment 1 (a); element 2 (b); element 3 (c); element 4 (d) (r_{yx} - distance between Y direction and axis X; r_{xy} - distance between X direction and axis Y)

With different loading options, the stress distribution in this element has an apparent symmetry. When the Y coordinate has a value of -250 mm or 250 mm (which determines the width of the “kerchief”), the presence of the most significant stresses is recorded. In the case of an increase in the X coordinate (which determines the height of the “gusset”), as it approaches element 4, the stress level gradually increases, and in the area close to element 4 ($X \approx 550$ mm), the calculated stresses are maximum.

Graphical interpretation of the calculated stress distribution on element 2 (top cover) shows the following (Fig. 4b). The pattern of stress distribution on this element is also symmetrical. As for the selected element 1, the maximum stresses are fixed in the case when the Y coordinate reaches the value of -250 mm or 250 mm. As the X coordinate increases, the stresses on element 2 first increase, then decrease, then gradually increase,

and finally increase sharply. At the value of the coordinate $X = 370$ mm, which determines the overlap of elements 1 and 2, the stresses decrease. This is due to a sharp change in the total cross-section of these two elements due to their permanent connection by welding. When the coordinate $X \approx 550$ mm, thus defining a place close to element 4, a significant increase in the voltage on element 2 was recorded.

Graphical interpretation of the calculated stress distribution on element 3 (bottom cover) shows the following (Fig. 4c). The stress distribution on this element is also symmetrical. But in contrast to the distribution of stresses on elements 1 and 2, the value of the Y coordinate -250 mm or 250 mm for element 3 determines the presence of the lowest stresses. As the X-coordinate increases, the stresses on element 3 first increase and then decrease. At $X = 550$ mm, the maximum stress values were recorded for the element under consideration.

Graphical interpretation of the calculated stress distribution on element 4 shows the following (Fig. 4d). At different loading values, the stress on the inner and outer surfaces of element 4 gradually increases with the increase in the Z coordinate, which determines the place of application of the external load. When the coordinate takes the value $Z \approx 750$ mm, determining the place of connection between elements 1, 2 and 4, the stress values are maximum. Moreover, the stresses on the inner surface of the element of element 4 are 25% greater than on its outer surface.

Thus, based on the study, it follows that the stress peak point is located at the junction of elements 1, 2, and 4.

5 Conclusions

Based on the research carried out, the following conclusions were obtained:

1. Comparative analysis of the results of the calculation of the stress-strain state at the selected reference point, obtained in the case of using the created finite element model of the device under consideration and its simplified calculation model, indicate their identity with a relative error of 2.5%, which confirms the adequacy the developed model and the reliability of the results of the conducted numerical simulation.
2. The stress peak point established during the study, located at the junction of elements 1, 2, and 4, allows a number of works to optimize the shaping of the connected elements and technological requirements when creating the connection itself. Given that the connection is welded, it is possible to recommend using additional strength elements at the junction or an increase in the height of the “kerchief”, which will increase the overlap between the elements and increase the area of the welds.
3. The obtained data provide a theoretical basis for installing warning sensors about the force state of the ship’s floating bollard at the place of the stress peak or in its immediate vicinity.
4. The use of the proposed system of control sensors will allow organizing service for the preliminary cleaning of ships from snow and ice in winter before locking.

References

1. Felski, A., Zwolak, K.: The ocean-going ships-challenges and threats. *J. Mar. Sci. Eng.* **8**, 41–50 (2020)
2. Ivanov, V., Pavlenko, I., Kuric, I., Kosov, M.: Mathematical modeling and numerical simulation of fixtures for fork-type parts manufacturing. In: Knapčíková, L., Balog, M. (eds.) *Industry 4.0: Trends in Management of Intelligent Manufacturing Systems*. EICC, pp. 133–142. Springer, Cham (2019). https://doi.org/10.1007/978-3-030-14011-3_12
3. Yudin, Yu.: Variable components of the effect of regular waves on the ship's hull. *Vestnik MGTU: works of Murman. state tech. un-that* **12**(3), 471–476 (2011)
4. Yang, S., Ringsberg, J.: Towards the assessment of impact of unmanned vessels on maritime transportation safety. *Realiab. Eng. Syst. Saf.* **165**, 155–169 (2017)
5. Bergdahl, L., Palm, J., Eskilsson, C., Lindahl, J.: Dynamically scaled model experiment of a mooring cable. *J. Mar. Sci. Eng* **4**, 5–12 (2016)
6. Johanning, L., Smith, G., Wolfram, J.: Measurements of static and dynamic mooring line damping and their importance for floating WEC devices. *Ocean Eng.* **34**, 1918–1934 (2007)
7. Martinelli, L., Ruol, P., Cortellazzo, G.: On mooring design of wave energy converters: the seabreath application. *Coast. Eng. Proc.* **1**, 3–18 (2012)
8. Pavlenko, I.: Static and dynamic analysis of the closing rotor balancing device of the multistage centrifugal pump. *Appl. Mech. Mater.* **630**, 248–254 (2014). <https://doi.org/10.4028/www.scientific.net/AMM.630.248>
9. Ivanov, V., Dehtiarov, I., Pavlenko, I., Kosov, I., Kosov, M.: Technology for complex parts machining in multiproduct manufacturing. *Manag. Prod. Eng. Rev.* **10**(2), 25–36 (2019). <https://doi.org/10.24425/mper.2019.129566>
10. Ivanov, V., Dehtiarov, I., Pavlenko, I., Kosov, M., Hatala, M.: Technological assurance and features of fork-type parts machining. In: Ivanov, V., et al. (eds.) *DSMIE 2019. LNME*, pp. 114–125. Springer, Cham (2020). https://doi.org/10.1007/978-3-030-22365-6_12
11. Tsukrov, I., Eroshkin, O., Paul, W.: Celikkol B. Numerical modeling of nonlinear elastic components of mooring systems. *IEEE J. Ocean. Eng.* **30**, 37–46 (2005)
12. Xu, Z., Huang, S.: Numerical investigation of mooring line damping and the drag coefficients of studless chain links. *J. Mar. Sci. Appl.* **13**(1), 76–84 (2014). <https://doi.org/10.1007/s11804-014-1235-0>
13. Trojanowski, P., Trojanowska, J.: Reliability of road transport means as a factor affecting the risk of failure – the transport problem case study. In: Ivanov, V., Trojanowska, J., Pavlenko, I., Zajac, J., Peraković, D. (eds.) *DSMIE 2021. LNME*, pp. 253–261. Springer, Cham (2021). https://doi.org/10.1007/978-3-030-77719-7_26
14. Trojanowski, P., Filina-Dawidowicz, L.: Diagnostic and repair centers locating methodology for vehicles carrying sensitive cargo. *Transp. Res. Procedia* **55**, 410–417 (2021). <https://doi.org/10.1016/j.trpro.2021.07.004>
15. Lasinska, N.: Hybrid management methodology for transport projects related to rolling stock. *J. Eng. Sci.* **8**(2), B7–B11 (2021). [https://doi.org/10.21272/jes.2021.8\(2\).b2](https://doi.org/10.21272/jes.2021.8(2).b2)
16. Trojanowski, P.: Comparative analysis of the impact of road infrastructure development on road safety – a case study. *Sci. J. Maritime Univ. Szczecin* 23–28 (2020). <https://doi.org/10.17402/436>
17. Spanos, P., Arena, F., Richichi, A., Malara, G.: Efficient dynamic analysis of a nonlinear wave energy harvester model. *J. Offshore Mech. Arctic Eng.* **138**, 40–49 (2016)
18. Chai, Y., Varyani, K., Barltrop, N.: Semi-analytical quasi-static formulation for three-dimensional partially grounded mooring system problems. *Ocean Eng.* **29**, 627–649 (2002)
19. Pascoal, R., Huang, S., Barltrop, N., Soares, C.: Equivalent force model for the effect of mooring systems on the horizontal motions. *Appl. Ocean Res.* **27**, 165–172 (2005)

20. Bate, K.: *Finite Element Methods*. Fizmatlit, Moscow (2010)
21. Pavlenko, I.V., Simonovskiy, V.I., Demianenko, M.M.: Dynamic analysis of centrifugal machines rotors supported on ball bearings by combined application of 3D and beam finite element models. *IOP Conf. Ser. Mater. Sci. Eng.* **233**(1), 012053 (2017). <https://doi.org/10.1088/1757-899X/233/1/012053>
22. Ivanov, V., et al.: Numerical simulation of the system “fixture–workpiece” for lever machining. *Int. J. Adv. Manuf. Technol.* **91**(1–4), 79–90 (2016). <https://doi.org/10.1007/s00170-016-9701-2>